Structural characterization by confocal laser scanning microscopy and electrochemical study of multi-walled carbon nanotube tyrosinase matrix for phenol detection†

Maria Guix,[ab] Briza Pérez-López,[a] Melike Sahin,[ac] Mònica Roldán,[d] Adriano Ambrosi[a] and Arben Merkoçi*[ae]

Received 14th January 2010, Accepted 13th May 2010
DOI: 10.1039/c000929f

A novel visualization methodology based on the use of immunofluorescence and Confocal Laser Scanning Microscopy (CLSM) was used to quantify and visualize tyrosinase enzyme within a MWCNTs matrix immobilized onto carbon based screen-printed electrodes. CLSM was shown to be an extremely powerful technique which allowed a clear visualization of the distribution of the enzyme within both the MWCNTs and carbon based layers and provided additional and useful morphological data for a better understanding of the interaction between biomolecules and electrode materials. Transmission Electron Microscopy (TEM) and Scanning Electron Microscopy (SEM) were also employed to fully characterize the system components. The proposed MWCNT/Tyrosinase matrix was applied to the detection of phenol, as an alternative biosensor material. Electrochemical analytical performances of the biosensor were investigated in order to determine the optimal fabrication design along with the enzyme stability. The biosensor based on the developed biomaterial matrix proved promising results in terms of cost, simplicity and analytical performance. A detection limit of 1.35 μM and a sensitivity of 47.4 μA mM^{-1} within a linear response range of 2.5 to 75 μM phenol were obtained. The biosensor performed well as a disposable device and could be stored in a refrigerator (−18 °C) without loss of activity for up to 2 months.

Introduction

Phenolic compounds are on the priority pollutants list of the European Community and the environmental Protection Agency of the United States because of their toxicity and persistency in the environment. They are commonly used in resin manufacture, and polymer and pharmaceutical products.[1] As they are compounds of particular environmental significance, it is important to be able to quantify and monitor them on-site.

Phenolic compounds are classically determined by gas chromatography and spectrophotometric analyses,[2] but these techniques are expensive, time-consuming and difficult to apply *in situ*. Electrochemical biosensors represent a promising alternative to the mentioned technique due to the extremely high sensitivity achievable, the simplicity of their use, very low cost and the fact that biosensors can be easily combined with miniaturized devices. Amperometric biosensors based on tyrosinase enzyme show high selectivity for phenol detection. Different matrixes such as carbon paste,[3] graphite epoxy composite,[4] sol–gel composite,[5] graphite-teflon electrodes,[6] glassy carbon electrodes[7] and screen-printed electrodes (SPEs)[8] have been reported. Screen-printing is a well-established microfabrication technology for the mass production of thick film electrodes and it is widely applied to build biological or chemical sensors,[9] which can be used without complicated sample pretreatment and therefore are suitable for on-site monitoring.[10]

Immobilization of the enzyme represents the crucial point in obtaining adequate sensitivities and overall stability of the biosensor. Different approaches, based on adsorption, covalent binding[11] or entrapment in polymers,[12] have been performed to achieve better immobilization of the enzyme. Nanostructured materials can be used to improve the incorporation of the enzyme into the sensing matrix and avoid its leaking. Better responses in terms of the biosensor performance are related to the intrinsic properties of the nanostructured materials used. Carbon nanotubes (CNTs) have unique structure-dependent electronic and mechanical properties[13] that when coupled with the specific recognition properties of enzymes provide important improvements in biosensors. Their advantages in electrochemical biosensing applications are mostly related to their capacity to mediate electron transfer reactions between electroactive species[14] and transducers thanks to their excellent electrical conductivity. Other exceptional properties of CNTs such as their mechanical strength and large surface area, which make them a potential linking bridge to attach biomolecules to the biosensor transducer, have been reported.[15,16]

[a]*Nanobioelectronics and Biosensors Group, Catalan Institute of Nanotechnology, UAB Campus, 08193 Bellaterra, Spain. E-mail: arben.merkoci.icn@uab.es; Fax: +34 935868020; Tel: +34 935868014*
[b]*Autonomous University of Barcelona, UAB Campus, 08193 Bellaterra, Spain*
[c]*Akdeniz University, Dumlupinar Boulevard, 07058 Campus Antalya, Turkey*
[d]*Microscopy Service, Autonomous University of Barcelona, UAB Campus, 08193 Bellaterra, Spain*
[e]*ICREA, Spain*

† Electronic supplementary information (ESI) available: Operational conditions in confocal studies, evaluation of possible autofluorescence of the materials and supplementary figures S1–S5. See DOI: 10.1039/c000929f

Incorporating carbon nanotubes into sensing devices generally requires the dispersion of CNTs in certain solvents so they can be processed into thin films or other applications.[17] To control the properties of the CNTs it is necessary to remove foreign nanoparticles that modify the physico-chemical properties of carbon nanotubes. CNTs processing permit the elimination of non-nanotube material, dispersion of individual nanotubes and chemical functionalization.[18] Purification of CNTs by sonication can induce sidewall[19] or end[20] functionalization, which is of interest for facilitating their manipulations.[21]

An accurate and extensive characterization of the CNTs based matrix is very important for understanding the improved response mechanisms and consequently a correct interpretation of the device responses. Although CNTs are usually characterized prior to application by electron microscopy (SEM and TEM), Raman spectroscopy, thermal analysis and absorption spectroscopy (UV-Vis-NIR), it is also important to evaluate their properties once they have been applied/integrated into a matrix where biological molecules (*i.e.* enzymes) will be included. Careful testing with these techniques provides important information on the morphology, distribution and possible linkages of CNTs that can lead to significant improvements in CNTs based biosensors. In addition to the above mentioned techniques, confocal laser scanning microscopy (CLSM) is emerging as an indispensable tool that can provide valuable information related to the distribution of the incorporated enzyme within the sensing matrix layer.[22]

CLSM can be useful for characterizing not only the outer layer of the biosensing surface but also its interior, and provide at the same time a relative quantification of the enzyme. These studies aim to obtain a better understanding and control of the structure, shape and composition of the CNTs based biosensing materials and could be of interest for further investigations including biofuel cells,[23] drug delivery[24] or biomarkers analysis,[25] between others. Step by step CLSM characterisations of the carbon nanotube and tyrosinase based sensor along the preparation and use in order to further relate its structural characteristics to the electrochemical behaviour are presented. The study has not been limited to the 3D visualization of the matrix, but also an extensively CLSM statistical study to evaluate material roughness and its effect on enzyme distribution has been performed. Enzyme distribution and aggregation effects considered of crucial importance on the electrochemical process have also been studied.

Experimental

Materials and equipment

The following materials were obtained from the respective suppliers and used as received, except where indicated: CNTs powders (Aldrich, Germany, 95% purity), tetrahydrofuran (Fluka, Spain), phenol (SigmaUltra, Spain, > 99.5%), tyrosinase from mushroom (Sigma; *BioChemika*, Spain, lyophilized, ≥ 2000 units/mg 93898), mouse anti-tyrosinase (Invitrogen, United States, unconjugated monoclonal antibody specific to human tyrosinase. Concentration: 100μg/200μl.), Alexa Fluor ® 488 (Invitrogen, Molecular Probes, United States), TWEEN 20© (Sigma, Spain).

Potassium phosphate buffer (PBS) of pH 6.5 was prepared with potassium phophate monobasic (Fluka), potassium phosphate dibasic anhydrous and potassium chloride in MilliQ water. TWEEN buffer was prepared with TWEEN 20© (Aldrich).

Electrochemical experiments were performed using a model CHI 660A electrochemical workstation from CH Instrument Inc., Austin, TX. All electrochemical experiments were performed in a system composed of an electrochemical cell with the introduced SPE that contains working, auxiliary and reference electrodes in a single strip. SPE were fabricated in a semi-automatic screen-printing machine DEK 248 (DEK International, Switzerland), and the materials used were polyester sheets (Autostat HT5 from McDermid Autotype), Acheson carbon ink (Electrodag PF407C), Acheson silver/silver chloride ink (Electrodag 6037SS), and Minico 7000 Blue insulating ink (Acheson Industries, The Netherlands). Scanning electron microscopic images (SEM) of SPE were obtained using a Hitachi S-570 (Hitachi Ltd, Japan). Observations were carried out using a Leica TCS SP2 AOBS confocal microscope (Leica Microsystems, Germany) for the roughness experiments, a Leica TCS SP5 AOBS confocal microscope (Leica Microsystems, Germany) for the 3D images and to evaluate the enzyme distribution, and an Olympus FluoView FV1000 (Olympus, Tokyo, Japan) confocal microscope to compare the fluorescence intensity of different electrode formulations under the same conditions (for more information on the working conditions of the confocal studies see the ESI†). Samples were observed on Mat-Teck culture dishes (Mat Teck Corp., United States).

Preparation and characterization of SPE and their modification with CNTs

Screen-printed microfabrication is based on the sequential deposition of a graphite ink, Ag/AgCl ink and an insulating ink on a polyester substrate. After each layer is deposited a drying process is carried out, which consists on keeping the polyester substrate at 90 °C for 15 min. Previously to their dispersion, CNTs were purified by stirring them in 2 M nitric acid at 25 °C for 24 h. Multiwalled CNTs used have a purity of 95%.[26] The working surface area of a bare SPE was modified by depositing a 7 μl drop of MWCNTs suspension (1 mg MWCNTs/1 ml THF) onto the working electrode surface, followed by a drying process at room temperature for 24 h. The characterization process of the working electrode surface was performed by SEM to check if a homogeneous distribution of CNTs over the surface was achieved. SPEs characterization was performed by SEM studies of the surface and profile of the working electrode. Electrodes were mounted on adhesive carbon films and then coated with gold. Profile images were taken from electrodes that were previously immersed in liquid N_2 and immediately cut with a knife.

Immobilization of tyrosinase onto the working electrode SPE

Tyrosinase was immobilized onto the electrode surface by physical adsorption. Tyrosinase was dissolved in 0.1 M phosphate buffer (PBS) at pH 6.5 (prepared with MilliQ water). Tyrosinase solution (1 mg Tyrosinase/50 μl PBS) was stirred during 1 h and deposited onto the working electrode surface,

which was followed by a drying process at room temperature during 3 h.

Immunostaining protocol of tyrosinase

The protocol followed for immunostaining the working electrode surface was based on first incubating the primary label mouse anti-tyrosinase (30 μg/ml) during 3 h at 30 °C in a thermo shaker. The sample was cleaned with TWEEN20 at 0.05% in order to remove the primary marker not specifically attached to the enzyme. The second incubation step with the secondary antibody anti-mouse IgG conjugated to Alexa Fluor® 488 (5 μg/ml) was carried out under the same conditions used for the primary marker. The sample was washed again with TWEEN20 and left to dry for an hour. Alexa 488 labels were excited with an Ar laser (488 nm) and detected in the 495 to 520 nm range. The autofluorescence of the materials used was also studied in the spectral range of interest.

Evaluation of the roughness of the sample

Several fields of the electrode surface were evaluated. CSLM in reflection mode and three-dimensional analysis (topographic image) to assess the different parameters of roughness were used. Roughness parameters were calculated according to DIN-EN-ISO 4287 (1997).[27] Average roughness (Pa; arithmetic average of the profile ordinates within the measured section), root mean square (Pq; root mean square value of the profile ordinates within the measured section), maximum values for the valleys (Pn, depth of the greatest profile valleys) and peaks (Pp; height of the highest profile peak) are measured.

Although CLSM has less resolution than SEM, it is not limited to the surface characterization of the materials. Being a non-destructive method it can provide quantitative information on the roughness and the relative surface-to-area value of the different electrodes evaluated.

Results and discussion

CNTs dispersion

CNTs must be dispersed into a suitable solvent in order to achieve their homogeneous distribution onto the working electrode surface. Chemical oxidation (by previously stirring CNTs into 2 M nitric acid at 25 °C for 24 h) and physical treatment (applying a sonication process at room temperature during 4 h) shorten the CNTs and lead to the partial oxidation of the CNTs to produce functional oxygenated groups at the open ends and defects along the sidewall.[28] Impurities and defects in CNTs were characterized by SEM microanalysis and showed that traces of iron (Fe), nickel (Ni) and potassium (K) from 0.5%, 1.6% and 1.5% were decreased to 0.1%, 0.9% and 0.4% after treatment with nitric acid.[29] CNTs were dispersed in THF (1 mg of CNTs/1 ml THF) during four hours by sonication.

The TEM image (see Fig. S1 of the ESI†) reveals a good dispersion of the CNTs in THF. At the same time, some impurities that are probably related to the remaining metals are observed in the different TEM images taken. Defects along the tubes can also be seen in addition to the impurities.

Working electrode characterization

There are many different ways to characterize surfaces and to compare them to each other. Visual comparison of SEM images represents the most common way. In addition, various roughness parameters have been previously identified as important to quantify different materials.[30] Surface characterization in terms of roughness and CNTs distribution was evaluated by taking SEM images of the electrode surfaces for both bare and MWCNTs modified SPEs (see Fig. 1A to C). The images of different areas (considering not only the working electrode surface, but also the insulator area, reference electrode and counter electrode) have been taken. These images (not shown) didn't demonstrate any effect of THF in terms of roughness. Profile images of the working electrode surface are shown in order to study the structure and roughness of the different layers that configure the membrane of a SPE modified with CNTs (Fig. 1D).

A more sponge-like structure of the MWCNTs modified surface (C2) in comparison to bare SPE surface (B2) can be observed. The cut view of the MWCNTs (Fig. 1D) clearly shows the MWCNTs layer deposited over the previous imprinted carbon layer. The evident roughness would be with interest for biosensing application due to the increased sensing area.

A more accurate quantitative study of the sensor surface is done by calculating several statistical data that correspond to the studied sensor surfaces using CLSM (using the reflection mode previously described). The average roughness (Pa), the root mean square (Pq), maximum values for the valleys (Pn) and peaks (Pp) of both bare and CNT modified SPEs are summarized in Table 1. These values clearly indicate that quantitatively SPE modified with CNTs have a higher average roughness and a higher maximum values for the valleys and peaks compared to the carbon surface of the unmodified SPE.

The CLSM data are in agreement with SEM images and confirm once again the increase of roughness, area, maximum values of valleys and peaks of the CNTs modified *versus* bare SPE.

Coupling CLSM with the specificity of immunostaining techniques has been proved to be a good technique for evaluating the distribution of biological species in certain matrixes.[31] Tyrosinase immobilization into the CNTs matrix can be evaluated by CLSM using optical sectioning through a material up to a 100 μm depth. Maximum height section studied was *ca.* 18.14 μm (corresponding to the electrode modified with CNTs). Taking several images of successive depth planes of the material allow three dimensional (3D) imaging of the matrix.

The possible autofluorescence of the different electrode constituents (*i.e.* polyester substrate and carbon ink) before and after applying the immunostaining protocol have been studied. The control of the possible autofluorescence coming from the different materials that constitute the biosensing area are also evaluated so as to avoid false positives. The used electrode materials didn't show any autofluorescence in the spectra of interest (results not shown). Consequently, the fluorescence of the studied sensors is only due to the presence of the tyrosinase in the different studied matrixes. This protocol allows the problems usually present in immunochemistry to be avoided. First, non-specific binding is prevented by using a non-ionic detergent

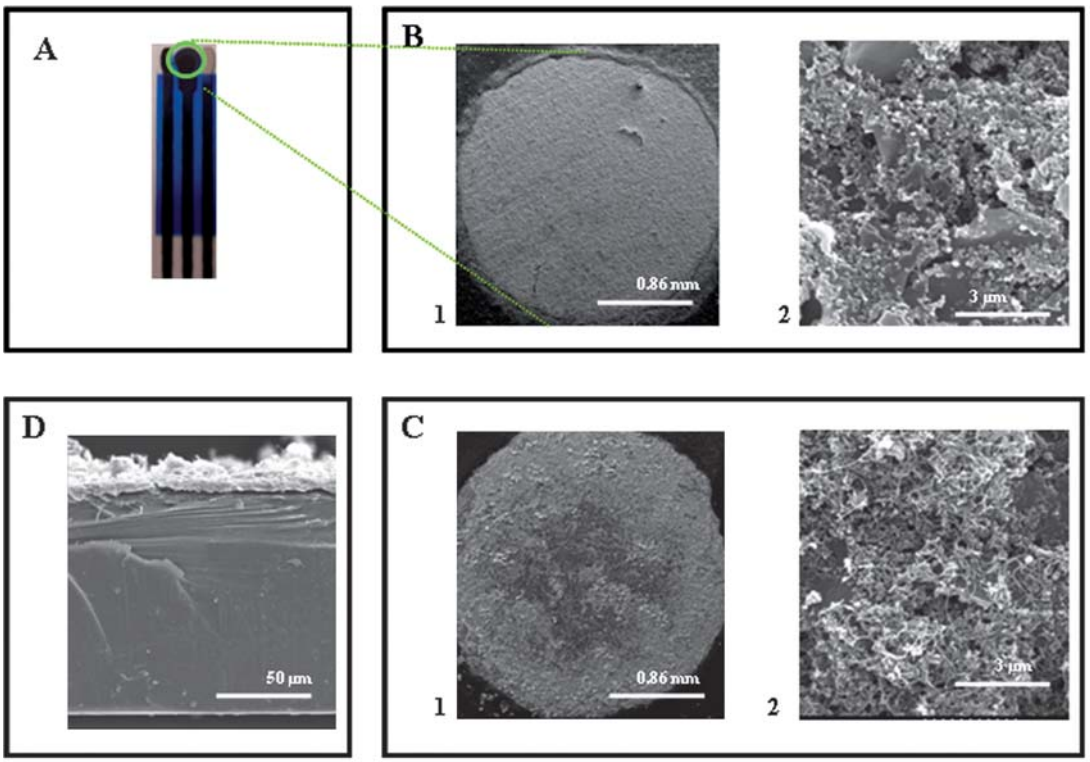

Fig. 1 Image of the SPE (A) where the working surface area evaluated by SEM is circled in green. SEM images of the working surface area of a bare (B) and MWCNTs (C) modified SPE at different resolutions: 0.86 mm (B1 and C1) and 3 μm (B2 and C2). In the case of SPE modified with MWCNTs, a suspension of 7 μl of MWCNTs dispersion (1 mg MWCNT/1 ml THF) was dropped onto the working electrode area and left to be dried at room temperature during 24 h. SEM image of the profile of SPE modified with MWCNTs (D) is also shown.

(TWEEN20) that removes the primary marker of the secondary label not specifically attached. By simultaneously combining temperature and agitation we prevented the extended incubation times, thus reducing the normal time of 48 h[31a] which can often provoke high background, to 3 h.

CLSM is suitable to study the enzyme distribution through the working electrode surface. An *in situ* 3D representation of this distribution can be seen in Fig. 2. A better distribution of tyrosinase onto the electrode surface as well as in depth is observed at the CNTs based SPE. Furthermore, it is possible to have been measured across all individual CLSM images of the stack. This value gives an idea of the sum of the total fluorescence in the frame scanned. As the fluorescence is proportional to the enzyme present in the sample, this integrated value can be related to the total enzyme adsorbed in this stack. Comparing the frame scanned for the bare and the modified SPE a quantity of the immobilized tyrosinase enzyme 1.96 times higher in the case of the MWCNTs modified SPE is found.

Additional information on the relation between the tyrosinase distribution and the roughness can be found by overlapping the signal obtained by the reflection mode and the fluorescence signal obtained in the same linear region of interest (ROI) (see Fig. 3). The graphics of the fluorescence *versus* the depth along the ROI (left Fig. 3 graphics) demonstrate that the enzyme distribution is directly affected by the roughness of the sample.

CLSM images (Fig. 2 & 3) including the corresponding 3D and ROI related graphics qualitatively demonstrate that tyrosinase is well-distributed within the surface and the depth of the CNTs based matrix.

A quantitative evaluation of the enzyme distribution through the sensor surfaces was also studied by using a Leica TCS SP5 CLSM with the AOBS (Acousto Optical Beam Splitter) yielding a $264 \times 264\ \mu m^2$ field. An x–y line is drawn at increasing z depths to provide information on the evolution of the grey level intensity with z as shown in Fig. 4 (lower part). Graphs (upper part at Fig. 4) show that in both cases enzyme aggregates are formed.

Table 1 Quantitative information over the roughness of different formulations evaluated by CLSM. Formulation evaluated were bare SPE and SPE modified with CNTs. Statistical data and its standard deviation are presented and consists of the average roughness (Pa), root mean square (Pq), maximum values for the valleys (Pn) and peaks (Pp). Seven fields for each surface (bare and CNTs modified) were studied using the reflection mode evaluated by DIN-EN-ISO 4287[26]

SPE	Pa	Pq	Pn	Pp
Bare	1.51 ± 0.25	2.06 ± 0.57	14.57 ± 1.58	13.49 ± 3.14
CNTs modified	2.23 ± 0.39	3.03 ± 0.45	18.14 ± 1.62	15.52 ± 1.74

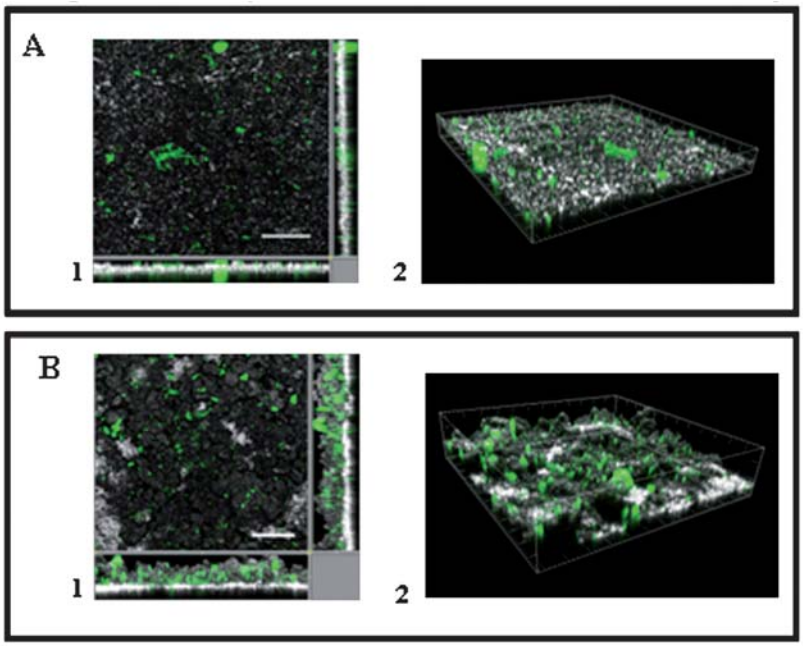

Fig. 2 CLSM images of the sensor surfaces. (A) Distribution of tyrosinase in the SPE carbon matrix (1) and its corresponding 3D confocal images (2). (B) Distribution of tyrosinase in the SPE CNTs matrix (1), and its corresponding 3D confocal images (2). Scale bar 50 μm. Experimental details as described in the text.

These aggregates are differently distributed depending on the matrix. The mentioned aggregates are related to wider and higher intensity bands observed in several *z* depths. Bigger but not homogeneously distributed aggregates can be observed in the case of the bare SPE (carbon based only) being a more homogenous distribution of the enzyme, with fewer and smaller aggregates for the CNTs matrix.

Electrochemical testing of SPE/MWCNT/Tyr

Tyrosinase has hydroxylase activity, by which phenol can be hydroxylated to catechol using molecular oxygen, and then oxidase activity that can catalyze the oxidation of catechol to o-quinone. At moderately negative potential the o-quinone product of phenol oxidation may be reduced electrochemically to

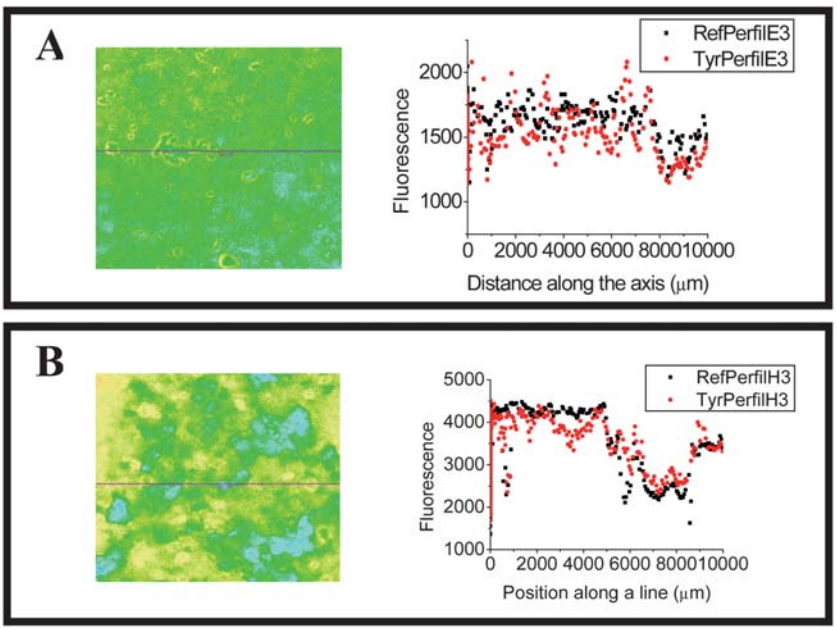

Fig. 3 Confocal micrographs of bare SPE (A) and CNTs modified SPE (B), with their corresponding graph. Fluorescence of the Alexa Fluor® 488 dye (pink) is overlapped with the signal obtained by working in the reflection mode (blue). ROI (linear region of interest) used for each surface is shown. Other experimental details as described in the text.

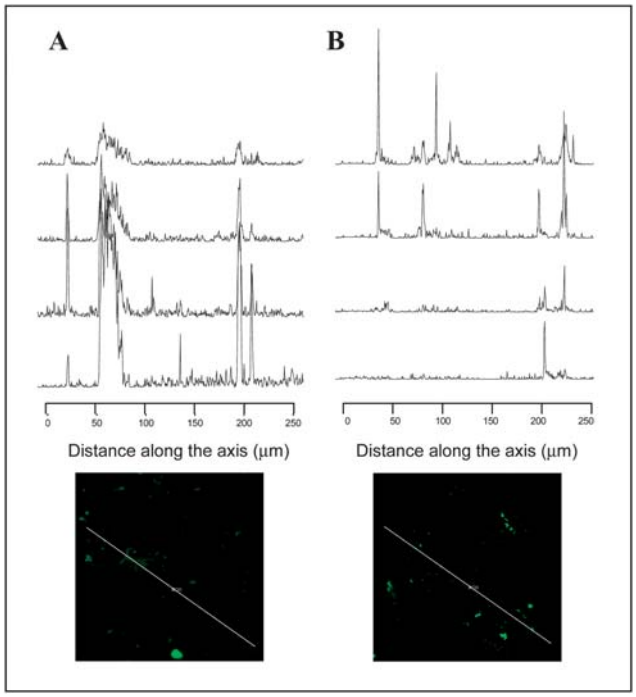

Fig. 4 Typical profiles of the grey level intensity along a given x–y line at increasing depths (step = 0.5μm) from $z = 20$ μm to $z = 60$ μm for the case of the enzyme immobilized in the bare SPE and the MWCNTs modified SPE. CLSM and other experimental conditions as explained in the text.

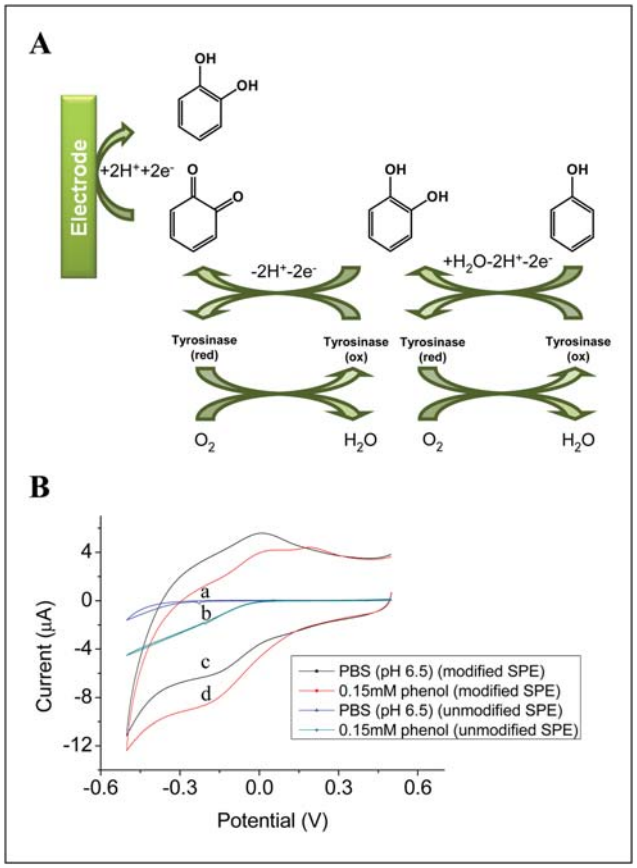

Fig. 5 Schematic diagram displaying the electrode reactions involved in the detection of phenol at the SPE surface using the tyrosinase enzyme (A). Cyclic voltammograms recorded for unmodified and modified SPE in 0.1 M PBS (pH 6.5) (B). Without (a), and with (b) 0.15 mM phenol addition with the SPE/Tyr biosensor; without (c) and with (d) 0.15mM phenol addition with the SPE/MWCNT/Tyr. Conditions used in the cyclic voltammograms: starting potential of 0.5 V; scan rate of 0.05 V/s and switching potential of −0.5 V. Reproducibility of peak potential, 11%; reproducibility of peak current, 39%.

catechol. Oxidation by the enzyme followed by reduction at the electrode may result in cycling between the catechol and o-quinone and yields a catalytically amplified current[6] (see Fig. 5A). Therefore, what is occurring at the electrode surface is the reduction of o-quinone to catechol (the working electrode acting as a cathode).

In order to understand the phenol detection mechanism using the developed MWCNT/Tyrosinase matrix cyclic voltammetry studies have been performed. The developed matrixes (SPE/Tyr and SPE/MWCNT/Tyr) are studied in the absence and presence of phenol substrate. While in the absence of phenol the SPE/Tyr did not give any significant response (see Fig. 5B, curve a) in the presence of phenol (Fig. 5B, curve b) a narrow shape CV characterized by a reduction peak (starting at −300 mV that goes toward more negative values) without reaching a plateau has been observed. A similar response to phenols at less negative potentials has also been previously reported.[6] SPE/MWCNT/Tyr displays a CV (Fig. 5B, curve c) with a broad shape and a peak at less negative potential (at −150 mV) in comparison to SPE/Tyr. In the presence of 0.15 mM of phenol an increase of the anodic current for SPE/MWCNT/Tyr (Fig. 5B, curve d) can be observed.

The working potential as well as enzyme loading have been studied. The working potential is a crucial parameter for the good operation of the biosensor. The optimum working potential is determined by two different methods. According to the first method, which is also the most reported, a hydrodynamic voltammogram is used to find the working potential (see Fig. S2 in the ESI†). This method consists in measuring the current obtained at different applied potentials for the same substrate concentration. A single addition of phenol is carried out before starting the experiment in stirring conditions. The variation of current *vs.* working potential is obtained and the optimal potential is determined according to the criteria of achieving a compromise between the highest current and the signal to noise ratio. According to the second method different chronoamperograms (current *vs.* phenol concentration for different working potential values) have been performed so as to better localize the working potential by also considering the phenol concentration level (see Fig. S3 in the ESI†).

The first method provides clear information on the best formulation according to the signal to noise criteria. The SPE/MWCNT/Tyr tyrosinase shows a higher current and a stable and practically without noise signal. The graphic of signal/noise *vs.* potential shows that the response to phenol for this matrix starts at −0.2 V. Taking into consideration the signal to noise ratio as well as the objective of working at the lowest potential value, a −0.2 V for SPE/MWCNT/Tyr was chosen as the optimal value for this first study.

Enzyme immobilization requires dissolving the tyrosinase enzyme. Enzyme was always solubilised in 0.1 M phosphate

buffer solution (PBS) pH 6.5, and the tyrosinase concentration used was 1 mg tyrosinase in 50 μl buffer. The responses to phenol detection were studied for two different concentration ranges of phenol: 2.5 μM to 25 μM and 25 μM to 250 μM. The first range is of special environmental interest. In the phenol concentration range of 25 to 250 μM the SPE/Tyr does not show any response while for the SPE/MWCNT formulation significantly enhances the current response (see Fig. S4 in the ESI†). The SPE modified with MWCNTs shows a stable and fast response for the first three additions, and starts to show saturation of the signal at the fourth addition due to the fouling of the electrode (Fig. 6). This fouling effect is mainly caused by the coupling reactions of o-quinone produced during phenol detection. This matrix is especially interesting for low phenol concentration detection, the high stability of the signal and the rapid response of the biosensor at the working range. Moreover, phenol concentrations over 2.5 and 25 μM are of special interest in the field of environmental analysis.

A stability study was carried out in order to evaluate the performance of the electrodes after being used (see Fig. 7). It can be observed that electrochemical activity of the electrode decreases from the first to the second day, probably due to the leaching of the enzyme from the surface of the SPE to the bulk of the solution. This would be due to the inefficiency of the immobilization method. Although the current tends to decrease after the second day, a considerable response was observed up to the seventh day. For the sake of comparability, the same conditions and stacks using an Olympus FluoView FV1000 microscope were considered (for more details see the ESI†). It is important to take into account that after electrochemical testing of the two matrixes (SPE with and without modification with CNTs), more aggregates were present in the SPE without CNTs (see Fig. 7).

SPEs modified with CNTs and tyrosinase with a concentration of 1 mg tyrosinase/50 μl buffer immobilized by physical adsorption were found to be the best conditions for phenol determination in batch. A range of phenol concentrations from 2.5 to 250 μM was studied. The analytical parameters related to our electrode formulation were a detection limit of 1.35 μM and a sensitivity of 47.4 μA mM^{-1} within a linear response range of 2.5 to 75 μM phenol (see Fig. 6). The limit of quantification, calculated as 10 times the concentration corresponding to noise level current, was found to be 4.51 μM; standard deviation of slope, 0.005 μM/μA; standard deviation of intercept, 0.008 μA. A shelf lifetime study (see Fig. S5 in the ESI†) was also performed and showed very promising results, with a shelf lifetime of 68 days while being stored in the refrigerator. This study consists in determining the lifetime during which the biosensor retains its quality under a certain set of storage conditions. This study was performed by keeping the SPEs modified with MWCNTs and tyrosinase in a refrigerator. The analytical performance of the electrodes was evaluated after 68 days and compared with the results obtained for the SPE checked on the first day of preparation. The analytical response of the electrodes after 68 days is practically the same as that of the preparation day.

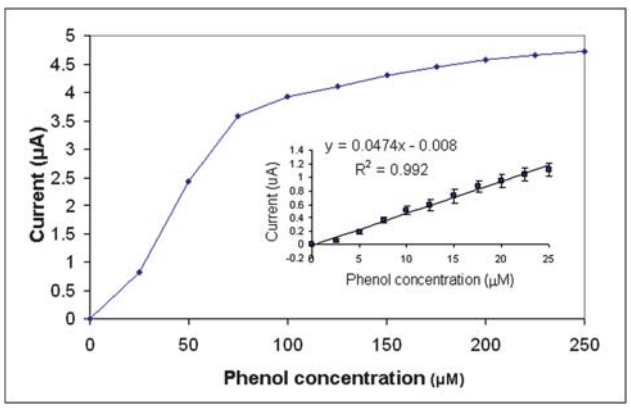

Fig. 6 Calibration plot corresponding to successive additions of 5 μl of a 2.5×10^{-5} M phenol solution into a 20 ml 0.1 M PBS (pH 6.5) during stirring conditions with a Tyr/MWCNT/SPE biosensor with tyrosinase concentration of 1 mg tyrosinase/50μl buffer. **Inset**: Calibration plot under the same conditions at the 2.5 to 25 μM range is shown.

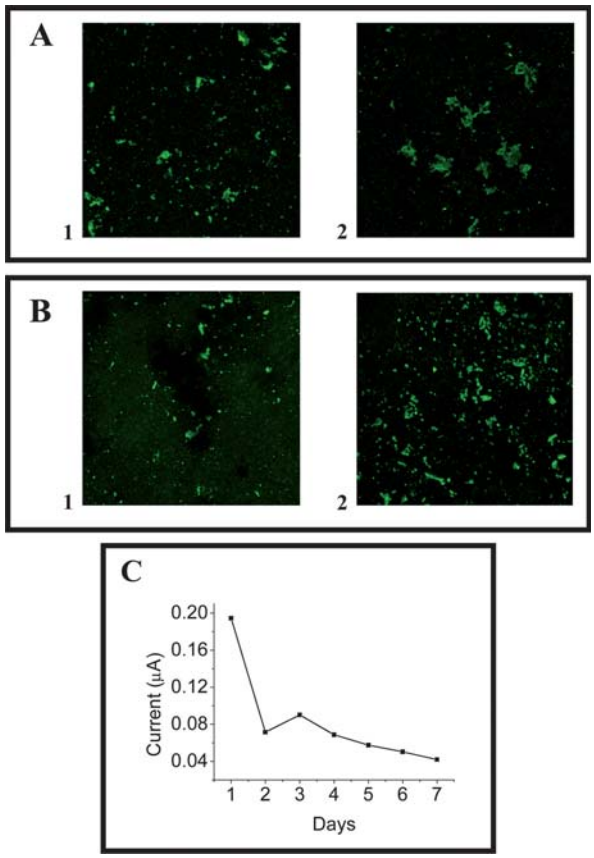

Fig. 7 *z*-projection of 20 stacks, separated by 0.5 μm, from bare SPE (A) and modified SPE with CNTs (B), both with the tyrosinase immobilized. Images A1 and B1 correspond to fresh electrodes not used for electrochemical measurements, and images A2 and B2 correspond to electrodes electrochemically tested after 7 days. Stability of the SPE/MWCNT with tyrosinase concentration of 1 mg tyrosinase/50 μl buffer toward a phenol solution obtained by adding 10 μl of a 5×10^{-6} M phenol solution into a 20 ml 0.1 M PBS (pH 6.5) during stirring conditions (C).

Conclusions

A promising MWCNTs and tyrosinase matrix (MWCNT/Tyr) applied onto the surface of a carbon based screen-printed

electrode (SPE) with interest to be used as phenol biosensor is developed. This matrix and the corresponding biosensor (SPE/MWCNT/Tyr) have advantages in terms of cost, simplicity, analytical performances while being used in phenol detection. SEM, TEM and Confocal Laser Scanning Mircroscopy (CLSM) studies had enabled a better understanding of the tyrosinase distribution within the MWCNTs based matrix. SPE without MWCNTs was compared to the SPE/MWCNT evaluating their roughness and how it interferes with the enzyme distribution by considering the enzyme distribution onto the surface as well as the depth of the carbon or MWCNTs matrix. Roughness has been qualitatively and quantitatively studied using SEM and CSLM. 3D images of CSLM demonstrate a better distribution of the enzyme onto the MWCNTs matrix while higher aggregate formation in the case of the bare SPE electrode have been visualized. The formation of aggregates is also observed after a certain period of use and is related to a loss of electrochemical activity.

In terms of electrochemical behaviour, the electrode presents a detection limit of 1.35 μM and a sensitivity of 47.4 μA mM^{-1} within a linear response range of 2.5 to 75 μM phenol was obtained. The developed biosensors performed well as disposable devices and could be saved in a freezer (−18 °C) for up to 2 months.

The obtained detection limit of the developed biosensor should be useful for monitoring phenol contamination in the case of accidental pollution, industrial effluents *etc*. The application of this biosensor in drinking water monitoring would need further improvements so as to achieve the European drinking water limits.

Acknowledgements

The financial support from the Spanish Ministry of Science and Innovation through project MAT2008-03079/NAN and pre-doctoral fellowship (BES-2009-023939 given to M. G.) are acknowledged.

Notes and references

1 S. E. Manahan, *Environmental Chemistry*; Lewis Publishers, Chelsea, MI, 1991.
2 V. Janda and K. Krijt, *J. Chromatogr., A*, 1984, **283**, 309–314.
3 (*a*) M. P. Byfield and R. A. Abuknestra, *Biosens. Bioelectron.*, 1994, **9**, 373–399; (*b*) L. Gorton, *Electroanalysis*, 1995, **7**, 23–45; (*c*) K. Kalcher, J. M. Kauffmann, J. Wang, I. Svancara, K. Vytras, C. Neuhold and Z. Yang, *Electroanalysis*, 1995, **7**, 5–22; (*d*) K. R. Rogers, J. Y. Becker and J. Cembrano, *Electrochim. Acta*, 2000, **45**, 4373–4379.
4 (*a*) B. Pérez and A. Merkoçi, *Analyst*, 2009, **134**, 60–64; (*b*) B. Serra, E. Mateo, M. Pedrero, A. J. Reviejo and J. M. Pingarrón, *Analusis*, 1999, **27**, 592–299.
5 (*a*) B. Wang and S. Dong, *J. Electroanal. Chem.*, 2000, **487**, 45–50; (*b*) Rajesh, W. Takashima and K. Kaneto, *React. Funct. Polym.*, 2004, **59**, 163–169; (*c*) J. Kochana, A. Gala, A. Parczewski and J. Adamski, *Anal. Bioanal. Chem.*, 2008, **391**, 1275–1281.
6 (*a*) B. Serra, E. Mateo, M. Pedrero, A. J. Reviejo and J. M. Pingarrón, *Analusis*, 1999, **27**, 592–299; (*b*) B. Serra, S. Jiménez, M. L. Mena, A. J. Reviejo and J. M. Pingarrón, *Biosens. Bioelectron.*, 2002, **17**, 217–226; (*c*) V. Carralero, M. L. Mena, A. Gonzalez-Cortés, P. Yáñez-Sedeño and J. M. Pingarrón, *Biosens. Bioelectron.*, 2006, **22**, 730–736.
7 (*a*) D. Shan, C. Mousty, S. Cosnier and S. Mu, *Electroanalysis*, 2003, **15**, 1506–1512; (*b*) M. A. Kim and W. Y. Lee, *Anal. Chim. Acta*, 2003, **479**, 143–150; (*c*) T. Zhang, B. Tian, J. Kong, P. Yang and B. Liu, *Anal. Chim. Acta*, 2003, **489**, 199–206.
8 (*a*) R. Solná and P. Skládal, *Electroanalysis*, 2005, **17**, 2137–2146; (*b*) M. R. Montereali, W. Vastarella, L. Seta and R. Pilloton, *Int. J. Environ. Anal. Chem.*, 2005, **85**, 795–806.
9 P. Fanjul-Bolado, D. Hernández-Santos and P. J. Lamas-Ardisana, *Electrochim. Acta*, 2008, **53**, 3635–3642.
10 (*a*) C. D. Chriswell, R. C. Chang and J. S. Fritz, *Anal. Chem.*, 1975, **47**, 1325–1329; (*b*) J. Poerschmann, A. Zhang, F. D. Kopinke and T. Pawliszyn, *Anal. Chem.*, 1997, **69**, 597–600.
11 M. R. Montereali, W. Vastarella, L. Seta and R. Pilloton, *Int. J. Environ. Anal. Chem.*, 2005, **85**, 795–806.
12 S. Sánchez, M. Roldán, S. Pérez and E. Fabregas, *Anal. Chem.*, 2008, **80**, 6508–6514.
13 Y. Degani and A. Heller, *J. Phys. Chem.*, 1987, **91**, 1285–1289.
14 X. Zhang, H. Ju and J. Wang, *Electrochemical Sensors, Biosensors and Their Biomedical Applications*, Elsevier, Amsterdam, 2007.
15 Y. P. Sun, L. F. Fu, Y. Lin and W. J. Huang, *Acc. Chem. Res.*, 2002, **35**, 1096–1104.
16 M. Meyyappan, *Carbon Nanotubes: Science and Applications*, CRC Press, Boca Raton, 2005.
17 (*a*) H. Luo, Z. Shi, L. Nangiang, G. Zhennan and Q. Zhuang, *Anal. Chem.*, 2001, **73**, 915–920; (*b*) J. Wang and M. Musameh, *Analyst*, 2004, **129**, 1–2.
18 U. Yogeswaran and S. M. Chen, *Anal. Lett.*, 2008, **41**, 210–243.
19 D. Tasis, N. Tagmatarchis, V. Georgakilas and M. Prato, *Chem.–Eur. J.*, 2003, **9**, 4001–4008.
20 J. Chen, M. A. Hamon, H. Hu, Y. Chen, A. M. Rao, P. C. Eklund and R. C. Haddon, *Science*, 1998, **282**, 95–98.
21 K. Gong, Y. Yan, M. Zhang, L. Su, S. Xiong and L. Mao, *Anal. Sci.*, 2005, **21**, 1383–1393.
22 J. Li, Z. Jiang, H. Wu, L. Zhang, L. Long and Y. Jiang, *Soft Matter*, 2010, **6**, 542–550.
23 (*a*) S. C. Wang, F. Yang, M. Silva, A. Zarow, Y. Wang and Z. Iqbal, *Electrochem. Commun.*, 2009, **11**, 34–37; (*b*) X. Li, H. Zhou, P. Yu, L. Su, T. Ohsaka and L. Mao, *Electrochem. Commun.*, 2008, **10**, 851–854; (*c*) Y. Yan, W. Zheng, L. Su and L. Mao, *Adv. Mater.*, 2006, **18**, 2639–2643.
24 (*a*) A. Bianco, K. Kostarelos and M. Prato, *Curr. Opin. Chem. Biol.*, 2005, **9**, 674–679; (*b*) K. Kostarelos, A. Bianco and M. Prato, *Nat. Nanotechnol.*, 2009, **4**, 627–633; (*c*) Z. Liu, A. C. Fan, K. Rakhra, S. Sherlock, A. Goodwin, X. Chen, Q. Yang, D. W. Felsher and H. Dai, *Angew. Chem., Int. Ed.*, 2009, **48**, 7668–7672; (*d*) W. Wu, R. Li, X. Bian, Z. Zhu, D. Ding, X. Li, Z. Jia, X. Jiang and Y. Hu, *ACS Nano*, 2009, **3**, 2740–2750.
25 X. Yu, B. Munge, V. Patel, G. Jensen, A. Bhirde, J. D. Gong, S. N. Kim, J. Gillespie, J. S. Gutking, F. Papadimitrakopoulos and J. F. Rusling, *J. Am. Chem. Soc.*, 2006, **128**, 11199–11205.
26 B. Pérez, M. Pumera, M. Valle, A. Merkoçi and S. Alegret, *J. Nanosci. Nanotechnol.*, 2005, **5**, 1694–1698.
27 ISO 4287. *Geometrical product specifications (GPS)-surface texture: profile method-terms, definitions and surface texture parameters, International Organization for Standardization*, Switzerland, 1997.
28 N. W. S. Kam, T. C. Jessop, P. A. Wender and H. Dai, *J. Am. Chem. Soc.*, 2004, **126**, 6850–6851.
29 G. Alarcón-Angeles, B. Pérez-López, M. Palomar-Pardave and M. T. Ramírez-Silva, *Carbon*, 2008, **46**, 898–906.
30 (*a*) M. Pohl and J. Stella, *Wear*, 2002, **252**, 501–511; (*b*) F. V. Antunes, A. Ramalho and J. M. Ferreira, *Int. J. Fatigue*, 2000, **22**, 781–788; (*c*) B. Işık, *Int. J. Adv. Manuf. Technol.*, 2008, **37**, 42–48.
31 (*a*) H. Liu and W. W. Y. Kao, *Mol. Vis.*, 2009, **15**, 505–517; (*b*) M. Chalal, F. Ehrburger-Dolle, I. Morfin, J. C. Vial, M. R. Aguilar, J. San-Roman, N. Bölgen, E. Piskin, O. Ziane and R. Casalegno, *Macromolecules*, 2009, **42**, 2749–2755.